https://www.doi.org/10.53964/jmn.2022002

https://www.innovationforever.com

Journal of Modern Nanotechnology

ISSN 2788-8118

Open Access

Research Article

Experimental Investigation of the Effect of Silica Nanoparticles on Interfacial Tension and Wettability during Low Salinity Water Flooding: A Micromodel Study

Shirin Safarzadeh[1*], Alberto Bila[2,3], Ole Torsæter[1]

[1]Department of Geoscience and Petroleum, Norwegian University of Science and Technology, Trondheim, Norway

[2]Department of Chemical Engineering, Eduardo Mondlane University (EMU), Maputo, Mozambique

[3]Centre of Studies in Oil and Gas Engineering and Technology, Eduardo Mondlane University (EMU), Maputo, Mozambique

***Correspondence to:** Shirin Safarzadeh, Department of Geoscience and Petroleum, Norwegian University of Science and Technology, Trondheim 7031, Norway; Email: Shirinsafarzadeh3@gmail.com

Received: November 26, 2021 **Accepted:** January 12, 2022 **Published:** March 31, 2022

Abstract

Objective: The present paper investigates the effect of nanoparticle concentrations on the interfacial tension and wettability during the low salinity water flooding (LSWF) at microscale.

Method: A wide range of LSW concentrations were prepared and investigated for their ability to modulate the interfacial tension with crude oil. The impact of salinity on the fluid-rock interactions was studied through contact angle measurements on water-wet, intermediate-wet and oil-wet glass substrates. Nanofluid systems at a fixed concentration of 0.1wt% were prepared by mixing the hydrophilic silica NPs with a wide range of LSW concentrations. Likewise, the impact of silica nanoparticles on the IFT was investigated.

Results: The fluids interactions results suggest that the lowest IFT value can be achieved at 5000ppm. Contact angle studies in all wettability systems indicated a negligible effect of water salinity on the wettability alteration. However, the presence of silica nanoparticles in low saline water significantly reduced the values of IFT and contact angle. Consequently, the wettability was altered to a more water-wet condition.

Conclusions: Oil displacement experiments in both water-wet, intermediate-wet and oil-wet glass micromodels indicated that LSW-augmented functional silica nanoparticles can offer enormous potential for improving oil recovery. A synergistic effect of LSW and the adsorption of nanoparticles at the interfaces appears to explain the improved oil sweep efficiency.

Keywords: low salinity, EOR, silica-nanoparticles, micromodel, interfacial tension, wettability alteration

Citation: Safarzadeh S, Bila A, Torsæter O. Experimental Investigation of the Effect of Silica Nanoparticles on Interfacial Tension and Wettability during Low Salinity Water Flooding: A Micromodel Study. *J Mod Nanotechnol*, 2022; 2(1): 2. DOI: 10.53964/jmn.2022002.

1 INTRODUCTION

The world's growing population is increasing energy demand. Energy consumption is vital for societies to flourish. According to a recent statistical review on the world energy, fossil fuels remain the main energy source, accounting for 84% of the global primary energy[1]. To meet the world demand for hydrocarbon resources, oil company's efforts center around maximizing the hydrocarbon fluids production from existing fields. In most oilfields water or gas injection is conducted to maintain the pressure gradients. However, a noticeable volume of oil is still left unproduced due to flow resisting forces. To put hydrocarbons trapped by capillary and viscous forces into a well stream, it is necessary to enter the tertiary recovery or enhanced oil recovery (EOR) stage. Low salinity water flooding (LSWF) is an enhanced oil recovery technique, in which diluted brine is injected into a reservoir to produce more oil. Bernard (1967) was the first who investigated the effect of low salinity water injection on recovery of oil from cores containing clays. In his experiments, both synthetic and natural water-wet cores (Berea sandstone) were flooded with waters of various salinities at ambient condition. He discovered when sodium chloride concentration of the injected water was varied between 1% and 15%, oil recovery and the pressure differential across the core remained unaffected. However, he observed more oil recovery as the NaCl concentration was decreased from 1% to 0.1% and the pressure difference along the core also increased[2]. Since then, LSWF has been applied at core scale, field scale, and micromodels by many researchers. As it is a simple, economical, and environmentally friendly method, it has received the oil industry's attention as a promising method. However, due to the complex interactions between oil, brine, and porous media, there is no agreement about the main mechanism(s) behind this EOR technique. The most proposed mechanisms for LSWF are fine migration, wettability alteration, interfacial tension reduction, increased pH, multicomponent ion exchange (MIE), double layer expansion, osmosis, and water diffusion[3]. The low salinity water injection design, in particular brine composition and amount of total dissolved salts (TDS), require careful experimental study to identify the key mechanisms and their effectiveness for a given reservoir. Moreover, the combination of nanofluid and low salinity water is a novel technique, which is believed to improve the efficiency of LSWF. The very small size (less than 100nm), large specific area and potentiality to alter the wettability towards water-wet render the nanoparticles (NPs) suitable candidates for being injected alongside water for EOR applications[4]. Silica nanoparticles are the most widely applied nanomaterials for EOR purposes. The widely accepted EOR mechanisms of silica nanoparticles are wettability alteration, IFT reduction[5]; other mechanisms may occur simultaneously such as, emulsion generation, disjoining pressure, and log-jamming effect[6-8].

Recently, the impact of nanoparticles mixed with low salinity water for EOR use has received attention in the petroleum industry. Hendraningrat & Torsæter (2016)[8] performed coreflooding experiments, using rock cores mostly consisting of quartz (83-93%). They observed that nanofluid's oil recovery efficiency is sensitive to water salinity content. According to their results, nanofluid injection with water salinity of 3000ppm (assumed as low-salinity water) showed negligible influence on oil recovery factor. However, when the water salinity was increased from 30 000 to 100 000ppm, higher incremental oil recovery was reported. Their results suggested that nanoparticle is most effective when it is injected along with increasing saline water content. It is well established that the thickness of the double-layer depends on the ion concentration in the surrounding water injection; increasing water salinity, the double layer compacts and strengthens the oil adsorbing forces. There may likely be a salinity threshold above which LSW-augmented nanoparticle injection is ineffective; this was not discussed by Hendraningrat & Torsæter (2016)[9]. Furthermore, the authors claimed that wettability alteration to more water-wet plays the major role in increasing oil production with water salinity of 100000ppm. Ebrahim et al. (2019)[9] found that mixing SiO_2 nanoparticles with LSW would increase the oil recovery by 4% of original oil in place (OOIP) over low salinity water injection in sand pack. Furthermore, Ebrahim et al. (2019) reported that adding silica nanoparticles to the LSW can decrease the contact angle more than LSW-free nanoparticles fluid. Moreover silica nanoparticles increased the viscosity of the injected water which improved the oil displacement efficiency and mobility ratio[10]. Dehghani & Daneshfar (2019) investigated the joint application of low-salinity water and nanoparticles by using both water-wet and oil-wet microfluidics. The authors argued that application of nanoparticles together with low salinity water can lead to wettability alteration, rendering the surface more water-wet[11]. Dehaghani & Daneshfar (2019) believed that, in a low-salinity environment, nanoparticle surface adsorption is the sole cause of surface wettability alteration. They added that structural disjoining pressure leads to a reduction in contact angle. However, the trend is somewhat unpredictable, suggesting that there is an optimum concentration of nanoparticles for the disjoining pressure mechanism to be effective.

The observations above suggest that nanotechnology can be successfully applied in conjunction with LSWF for

EOR. However, the EOR mechanisms underlying LSWF-augmented nanoparticles should be better understood.

In this paper, the effect of silica nanoparticles on interfacial tension and wettability during low salinity water flooding was studied. The effect of brine concentration and NPs on interfacial tension, contact angle and incremental oil recovery in systems with different wettability states has been discussed.

2 MATERIALS AND METHODS

2.1 Porous Media

Glass micromodels were used to visualize fluids flow in porous media. There are several reasons why microfluidics were chosen as porous media. First, it is feasible to monitor fluid flow directly. Furthermore, it is quicker than conventional core flooding experiments and use small volume of fluids. The disadvantages are that micromodels have two dimensions and pores are made of borosilicate glass instead of real rock materials, thus not capturing all physics occurring during EOR experiments. Moreover, it could be difficult to upscale the fluid flow behavior from microfluidics to reservoir rock[12]. Enhanced oil recovery chips are designed in three categories consisting of physical rock network, random network, and uniform network. In this study, microchips with physical rock network were used and it is shown in Figure 1. This kind of microchips with random rock shape structures mirror the actual porous media as much as possible. Microfluidic chips were initially water-wet and purchased from Micronit Micro Technologies. Each end of the glass micromodels is provided with inlet and out- let holes to allow for the injection and exiting of fluids. The main characteristics of the microfluidic chip are given in Table 1.

2.2 Oil Phase

In this work, a degassed crude oil from a field in the North Sea was used. The oil was filtered three times with a 5m filter paper to avoid blockage problems in the microfluidic chips. The crude oil is classified as light to medium sample. The measured density and viscosity at room temperature were 0.898g/cm^3 and 52.4mPa. s. Pycnometer was used to measure the density while a Rotating viscometer (Brook-field, LVDV/II+ P) was used for the viscosity. The total acid number (TAN) of the crude oil was relatively high, about 2.9mg KOH/g. Table 2 shows the SARA (Saturates, Aromates, Resins, Asphaltenes) analysis performed on the dead oil sample.

2.3 Low Salinity Water

Certain amount of salts were dissolved in distilled water to obtain a similar composition to that from the North Sea, with total dissolved salts (TDS) of 38 318ppm. The chemical composition of the prepared synthetic seawater (SSW) is shown in Table 3. The synthetic seawater had a density of 1.0254g/cm^3 and viscosity of 1.03cP at room temperature. Studies on the formation water composition from the Norwegian Continental Shelf (NCS) shows that the composition can be different from one field to another. In the North Sea, the formation water mainly consists of Na-Cl and the salinity ranges from 2500 to 212, 000 mg/kg[14]. In this work, the formation water was prepared with composition similar to that of a field from which the crude oil sample was taken. This synthetic seawater is then used as the interstitial water in micromodel chips.

Low salinity water (LSW) was prepared at different salinities. The composition of LSW samples and SSW were the same to tackle incompatibility issues between the injected phase (low-saline water) and formation water.

2.4 Nanofluids

The hydrophilic silica nanoparticles (AEROSIL) were provided by Evonik Industries as suspended particles in the liquid solution (AERODISP®). Their properties are presented in Table 4. The solutions of nano particles were diluted in water with the salinity of 0, 500 and 38,318ppm at a concentration of 0.1wt%. The resulting solutions of nanoparticles are referred to as nanofluid 1, 2 and 3, respectively (see Table 5).

2.5 Experimental Methodology

All experiments were performed at the NTNU reservoir engineering laboratory. In this work, the effect of salinity and nanoparticles dispersed in LSWF was investigated in terms of wettability alteration, interfacial tension measurement and displacement efficiency. Prior to any experiment, the stability of the prepared nanofluid system was evaluated. Finally, the oil recovery tests were carried out on a glass micromodel.

2.5.1 Interfacial Tension Measurement

IFT between crude oil and aqueous nanofluid solutions with different salinities was measured by pendant drop method at ambient conditions. the use of pendant drop technique offers several advantages. It is reliable, fast, straightforward and needs small amount of fluids[16]. A drop shape analyzer, KRÜSS DSA100S, with the innovative software called ADVANCE were used to measure IFT. The fitting curve to the crude oil drop hanging from a needle required to compute the IFT is based on Young-Laplace Equation 1:

$$\Delta P = \sigma\left(\frac{1}{R_1}+\frac{1}{R_2}\right) \qquad (1)$$

Where ΔP is the pressure difference across the interface of two immiscible fluids and R_1 and R_2 are the principal radii of curvature. A J-shaped needle with inner diameter of 1.0047mm deployed to make a drop of crude oil at its tip is surrounded by aqueous phase is shown in Figure 2. Twenty minutes after generating the oil drop in the aqueous phase sufficed to attain an equilibrium between the phases; then the equilibrium IFT value was recorded.

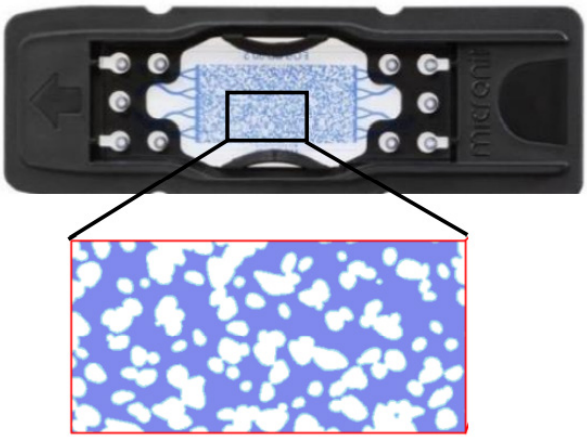

Figure 1. Microchip with physical rock network[13].

Table 1. Microfluidic Chip Characteristics

Characteristic	Value
Chip material	Borosilicate glass
Chip dimensions	45mm×15mm×1.8mm
Network dimension	20mm×10mm×0.02mm
Chip porosity	57%
Chip permeability	2.5 Darcy
Chip pore volume	5.7μL
Network pore volume	2.3μL

Table 2. SARA Analysis for Crude Oil (wt%)

Saturates	Aromates	Resins	Asphaltenes
66.21	25.78	7.69	0.32

Table 3. Chemical Compositions of Synthetic Seawater in 1 Liter Distilled Water[15]

Salt Components	Chemical Formula	raction (wt.%)
Sodium Chloride	NaCl	74.4
Potassium Chloride	KCl	1.85
Sodium Hydrogen Carbonate	$NaHCO_3$	0.57
Sodium Sulphate	Na_2SO_4	10.62
Calcium Chloride Dihydrate	$CaCl_2$ $2H_2O$	4.24
Magnesium Chloride Hexahydrate	$MgCl_2$ $6H_2O$	8.25

Table 4. Properties of NPs in Distilled Water

Sample	Concentration (wt%)	Particle Size (nm)
SiO_2 (sol-gel- anionic)	26	32

Table 5. Properties of NPs Suspended in Synthetic Seawater at Ambient Condition

Nanofluid (NF)	Concentration (wt%)	TDS (ppm)	P (g/cm3)	μ (cP)
NF 1	0.1	0	0.999	0.969
NF 2	0.1	5000	1.002	0.954
NF 3	0.1	38318	1.025	0.991

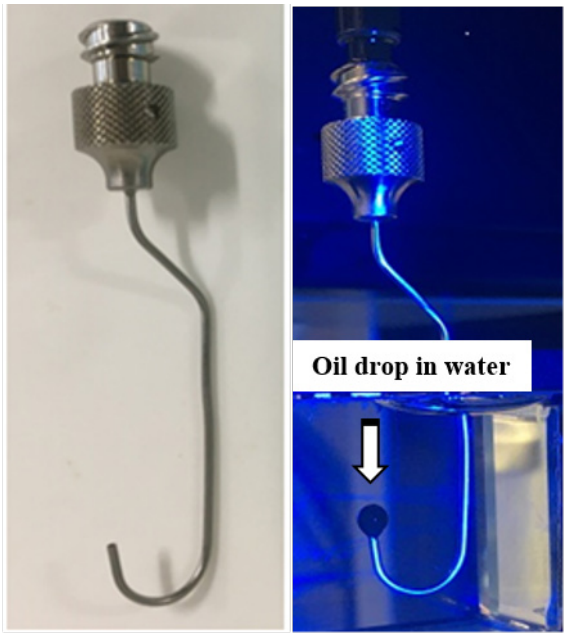

Figure 2. Left: J-shaped needle; Right: crude oil drop surround by aqueous phase.

2.5.2 Contact Angle Measurement

Similar to IFT measurement, KRÜSS DSA 100S apparatus was used to measure static contact angle at ambient temperature and pressure. Glass substrates played the role of solid surface. The initial wettability of these glasses was water-wet.

Hydrocarbon-soluble siliconizing fluid (Surfasil TS-42800, Thermo Scientific) was used to change the wettability of the substrates. Surfasil has a short chain, consisting of dichlorooctamethyltetrasiloxane; when it is applied to a glass surface, the unhydrolyzed chlorines present on the chain react with silanol groups on the glass surface, forming a neutral or hydrophobic surface, depending on the concentration, film over the entire surface[17]. SurfaSil was diluted in heptane at a concentration of 1v/v % and 0.05v/v % to change the wettability towards oil-wet and intermediate-wet states, respectively[15].

Depending on the measuring range, different fitting methods are available to measure the contact angle, namely circle method, conic section method, polynomial method, and Young-Laplace-Fit. Table 6 shows which method works better for modeling the drop shape based on the measuring ranges. In this regard, Young-Laplace fitting method was selected as the fitting technique in the ADVANCE software. All measurements were recorded after there was no further changes in the observed contact angle, which took about two hours for each measurement.

2.5.3 Nanoparticles Size Measurements

The stability of NPs in the injected fluid for EOR purpose is of high importance. In this regard, after diluting nanofluids in three water samples with the salinity of 0, 500 and 38,318ppm at a concentration of 0.1wt%, the NPs average diameter size was measured to verify if any aggregation has occurred. After 120 seconds, the sample in the Malvern Zetasizer Nano apparatus reached equilibrium. Afterwards, for each sample 36 measurements were performed, and the average value was recorded. The average diameter size of nanoparticles, before and after dilution in water with different salinities are summarized in Table 7. The small differences show that nanoparticles have remained relatively stable and dispersed, and no aggregation was observed.

2.5.4 Flooding Experiments

Figure 3 shows the schematic of micromodel setup used for secondary oil displacement experiments by LSW and nanofluids. The setup consists of a Harvard apparatus pump 33DDS (Dual Drive System) and single- use syringe with capacity of 5 ml (HENKE-JECT) which was horizontally established on the pump and connected to the microchip through tube lines (TUB0288). Ferrules were used to connect the tubing with the chip holder (Fluidic Connect PRO, Micronit) to secure the connection and avoid possible leakage. The other end of the microchip was connected to the glass tube test via tube lines to collect the effluent. For data acquisition, microscope (SZX7, Olympus) and digital camera.

(UC90, Olympus) with a resolution of 3384x2708 pixels attached to the microscope lens were implemented. Each pixel was equal to 0.00369mm. Olympus Stream software was installed on the computer to acquire the images during the experiments.

The glass micromodels were initially water-wet. Figure 4A shows oil and water within the pores of a glass surface; a thin layer of water is in direct contact with the substrate and prevents oil phase (brown) from adsorbing on the pore

Table 6. Recommended Fitting Method According to the Measuring Range[18]

Fitting Methods	Circle Method	Conic Section Method	Polynomial Method	Young-Laplace-Fit
Assumed drop shape	Circular arc	Ellipse	No prior assumption	Ideal sessile drop oblate by its own weight
Measuring Range				
0 to 20°	√			
10 to 100°		√	√	√
100 to 180°			√	√

Table 7. Average Diameter Size of NPs Before and After Dilution

Sample	Initial Diameter Size (nm)	Final Diameter Size (nm)	Differences (%)
NF 1	32	34.67	8.35
NF 2	32	34.58	8.06
NF 3	32	34.35	7.38

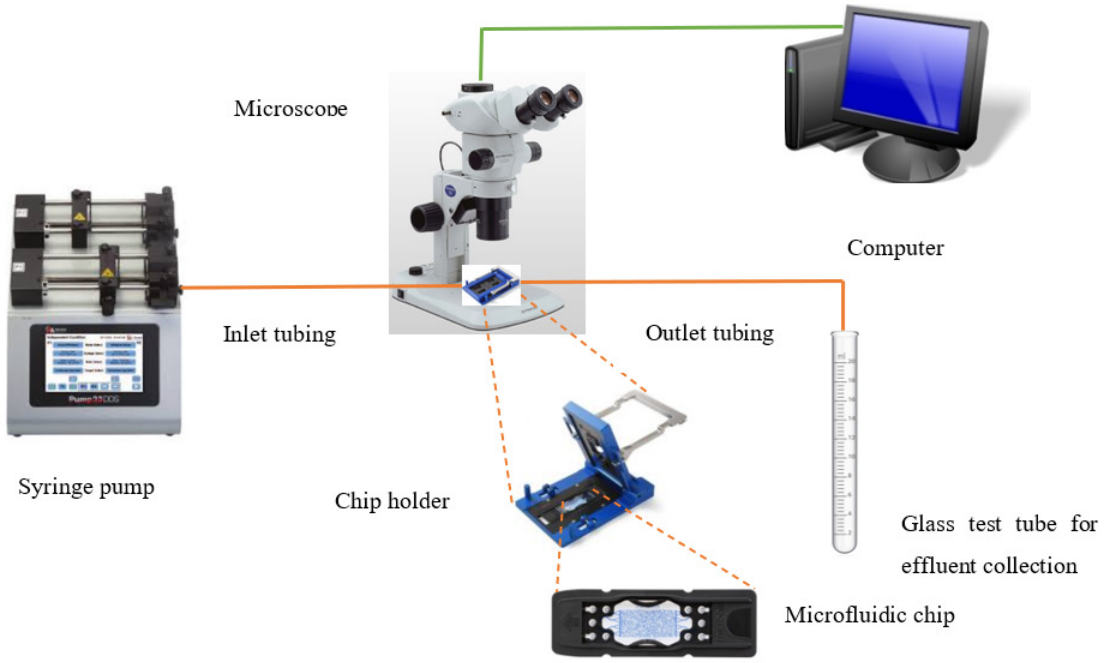

Figure 3. Schematic of micromodel setup.

walls. In order to monitor the impact of wettability state on the oil recovery, wettability of glass substrates were altered to intermediate-wet and oil-wet by the following procedure: a dry and clean microfluidic chip was injected with the hydrocarbon soluble siliconizing fluid; afterwards the microchip was respectively injected with heptane and methanol. Finally, the microchip was placed in the oven for drying at 80 °C for 24 hours[15]. Figure 4B illustrates an oil-wet microchip, which was flooded with synthetic seawater, followed by crude oil. One may notice that oil droplets are fully adsorbed on the pore walls, while surface is reluctant to adsorb water.

After changing the microchip's wettability to neutral- and oil-wet, the chip was mounted on the configured micromodel (see Figure 3). The air in the system was removed using a vacuum pump with the inlet valve closed. When the pressure of the system dropped below 40mbar, the vacuuming procedure was stopped. In the next step, the inlet valve was opened and synthetic sea water (38,318ppm) was injected followed by crude oil injection. Oil injection was carried out until there was no more water production, that is 100% oil stream in the effluent collector. At this stage, the initial oil and water saturation were achieved, and the system was ready for EOR experiments. In this study, the injection rate for all tests was constant at 0.1μL/min, corresponding to an average rate for a real oil field (1.26m/day). Nano fluids with different brine concentration were injected (see Table 5 and Table 8). To reproduce the results, the EOR displacement tests were performed twice for each nanofluid system, and average

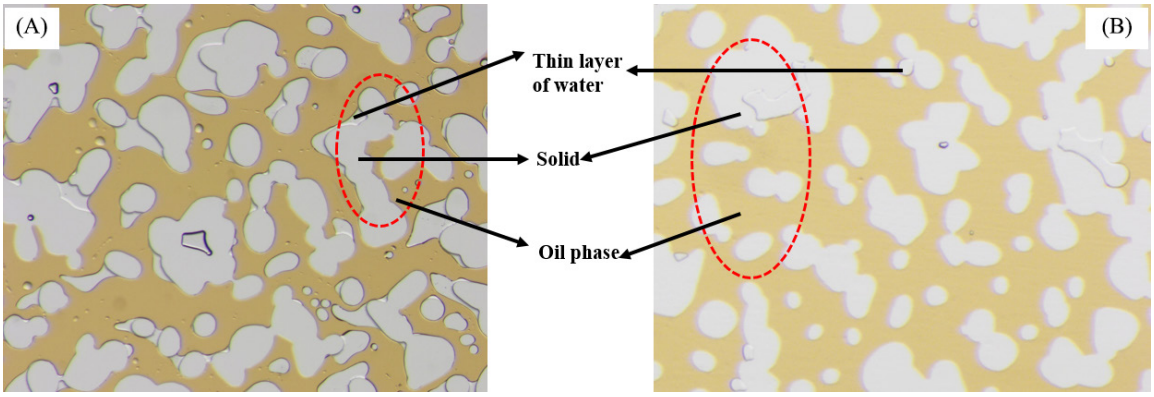

Figure 4. Sections of the micromodel fully saturated with crude oil at Swi. A Initially water-wet microchip; B Oil-wet microchip.

values reported.

All experiments were carried out until there were no further oil production. This was achieved about eight hours on average. The dimension of rock chip network was $20\times10mm^2$ (see Table 1), however, our camera was able to cover 77.5% and 100% of the length and width of the chip network, respectively. To be consistent, for all experiments an analyzing window with the dimension of $15.5 \times 10mm^2$ was selected which was the whole possible area. The corresponding pore volume to the covered area in this study was 1.78μL. To remove the capillary end effect of inlet and outlet, the set up was arranged in a way that microscope did not cover neither inlet nor outlet and photos were taken every 1 minute and 47 seconds (0.1 pore volume), which allowed to monitor oil saturation changes during the flooding precisely. A "for loop" Python code (open-source software, Python 3.7) was written to crop the edges of the microchip when it was necessary. In the next step to improve the quality of photos, particularly brightness and contrast, bandpass filter available in ImageJ software was applied. Afterwards the recorded images during the flooding were segmented to binary images by using MATLAB code and water saturation, oil saturation and recovery factor as a function of time was calculated. For instance, Figure 5 shows the binary image of an oil-wet microchip saturated with oil and synthetic sea water. Both aqueous phase and glass are shown by black, while oil phase is the white area.

3 RESULTS AND DISCUSSION

3.1 IFT Measurement

In this section, we investigate how the interfacial tension varies with salinity. Accordingly, the optimal brine concentration at which the minimum IFT can be obtained is evaluated. The impact of nanoparticles presence on IFT between aqueous and oil phase was also studied. The IFT results are presented in Table 9. and are referred to as equilibrium IFT values. Equilibrium IFT values were reached after 20 minutes. Figure 6 illustrates crude oil drop hanging from a needle submerged in brine solutions with different salinities.

For brine concentration from 0 to 10000ppm, which can be assumed as low salinity range, the IFT values varied between 12 and 17.64mN/m. To recognize the optimum concentration, at which the minimum IFT occurs, the equilibrium IFT between crude oil and low salinity water samples versus brine concentration is plotted in Figure 7. Looking at the details, it is clear that the highest IFT stands for a system in which oil and distilled water are in contact. However, after adding salts to the distilled water, IFT witnessed a sharp downward trend until 5000ppm. The optimum salinity is 5000ppm at which the lowest value of the equilibrium interfacial tension was recorded. In addition to low salinity water samples, IFT between high-saline brine (synthetic seawater (38318ppm) and its half-diluted sample (19159ppm) and crude oil is also plotted in Figure 7. Further addition of salts to 19159ppm, interfacial tension witnessed a downward trend and finally it remained steady. In order to explain the reason behind the observed trend, it is important to consider the effect of presence of asphaltene and resin in the crude oil. Hydrocarbon (hydrophobic) and the polar (hydrophilic) groups are present simultaneously on asphaltene and resin molecules, which make them behave like surface-active agents. Consequently, the system of interest is thermodynamically stable (minimum free energy or maximum entropy), if these natural surfactants are amassed at oil/water interface[20]. The IFT is related to the chemical activity of the present components in the binary liquid-liquid system through the Gibbs adsorption Equation 2[20–22].

$$d\sigma = -RT\Gamma d\ln C \qquad (2)$$

Where dσ is the change in the IFT of the solution, R is the universal gas constant, T is the absolute temperature, and Γ and C are the surface excess concentration and bulk concentration of surface-active agents respectively.

Figure 7 shows that at low brine concentration (0-5000ppm), interfacial tension is decreasing as a function of brine concentration. This trend can be attributed to the salt-in effect. Adding salts at low concentration leads to diffusion of natural surfactants from oleic phase to the interface, which makes the water/oil interface rich in asphaltene and resin.

Table 8. Properties of Water Samples

TDS (ppm)	ρ (g/cm^3)	μ (cP)
0	0.999	0.888
5000	1.0025	0.937
10000	1.0075	1.027
19159	1.0128	1.024
38318	1.0254	1.03

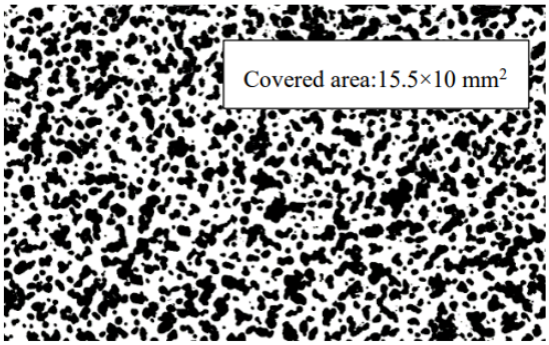

Figure 5. Binary image of an oil-wet microchip.

Table 9. IFT Values Between the Crude Oil and Brines with Different Salinities at Ambient Condition

Brine (ppm)	000000	1000	2000	3000	4000	5000	6000	7000	8000	9000	10000	19159	38318
IFT (mN/m)	17.64	15.99	13.34	15.36	14.06	12	12.05	13.54	13.85	13.82	14.08	8.84	8.38

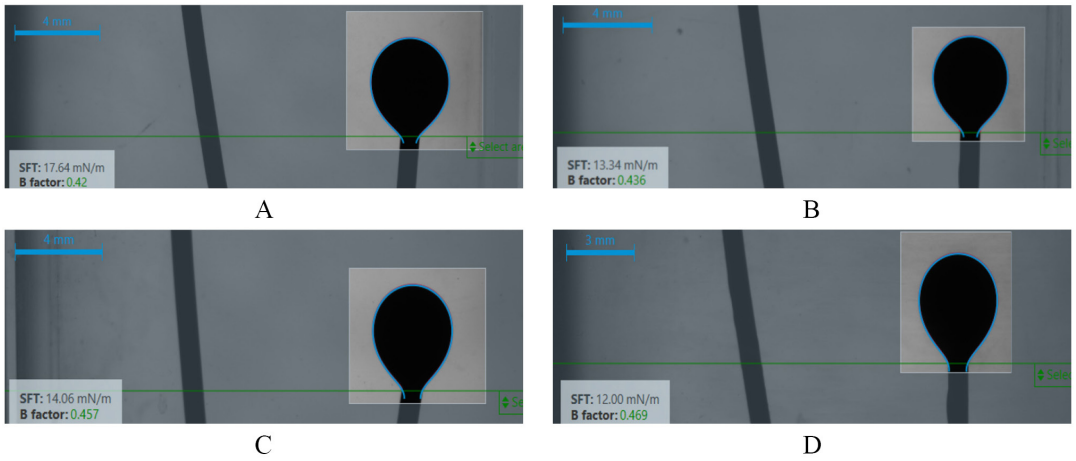

Figure 6. Interfacial tension measurement between crude oil and brines with different concentrations: A distilled water B 2000ppm C 4000ppm D 5000ppm. The relationship between the gravitational force and the IFT is expressed by the shape parameter, known as B factor[19].

Consequently, surfactant dominates the salt effect and IFT reduction occurs. Conversely, with further enhancement in the amount of salt, the cations concentration near the interface intensifies and water molecules cannot support the polarity of both added ions and natural surfactants (asphaltene and resin). Hence, these surface-active agents are forced to turn back to the oil phase. This phenomenon is called salting-out effect, which leads to higher interfacial tension after optimum salinity. In fact, according to Gibbs absorption equation for a binary system, due to higher brine concentration in the bulk phase than at the interface, the surface excess concentration of salts becomes negative and makes dσ positive which means higher IFT. At very high concentration of salt, strong affinity of divalent cations such as Mg^{2+} and Ca^{2+} towards the oxygen in the resin, alleviates the salting-out effect[23]. As a result, IFT reduces at high brine concentration and finally stabilizes over the range of 10000 to 38318ppm.The presence of nanoparticles (NPs) in the aqueous phase is another factor which can affect the behavior of the oil and water IFT. In fact, one of the main purposes of involving nanoparticles in EOR techniques is their ability to decrease the interfacial tension of the

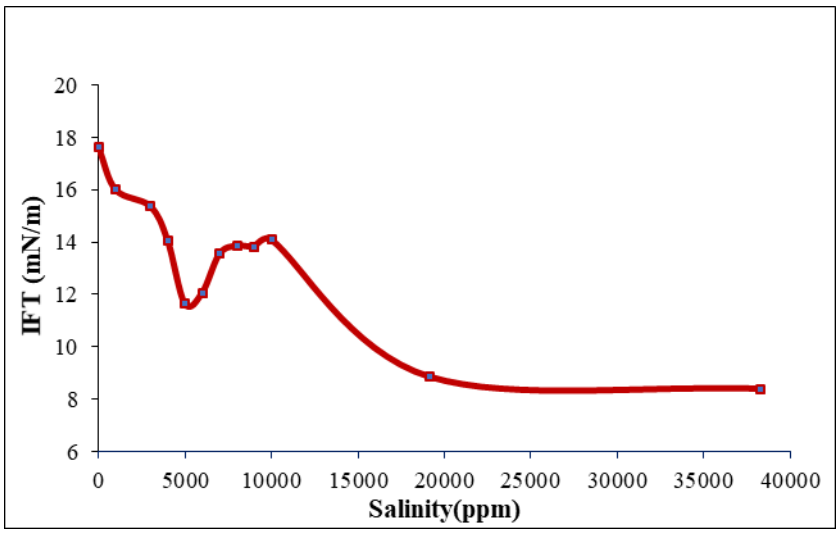

Figure 7. Interfacial tension variation over a wide range of salinity (0-38318ppm).

reservoir flowing fluids. In this work, silica nanoparticles were added to water with different amount of total dissolved salts (TDS) at a concentration of 0.1wt%. The presence of nanoparticles reduced the interfacial tension in all cases considerably. Generally, introduction of NPs to the system reduced the IFT between crude oil and water by 42.6 % to 51.1% (see Table 10 and Figure 8).

3.2 Contact Angle Measurement

In both intermediate-wet and oil-wet systems, the contact angle revealed a weak dependence on salinity in the aqueous phase. In other words, for a system including glass substrates, brine and crude oil, wettability of the glass was independent of the brine concentration (see Figure 9). To examine the reliability of the method used for measuring the contact angle, after EOR flood experiments, the contact angles were also measured at several points of the microchip, using ImageJ software. For example, Figure 10A shows contact angle measured on intermediate-wet glass substrates, crude oil and distilled water which is 105.1°. Figure 10B depicts a section of an intermediate-wet microchip flooded with distilled water. The average contact angle of these measurements was 101.96°. These results show the viability of the contact angle measurement with Young-Laplace fitting method.

Now let us investigate the impact of NPs on the contact angle. Increasing the water-wetness of the surface leads to higher ultimate oil recovery[24,25]. In this regard, using silica NPs have shown highly promising results in decreasing contact angle and consequently rendering a more water-wet surface. In this work, silica nanoparticles were added to water with different salinity with a constant concentration of 0.1wt% at room temperature. The recorded results showed a significant decrease in the contact angle and all systems shifted towards water-wet.

Intermediate-Wet System: Overall, introduction of NPs to the intermediate-wet system reduced contact angle by 38.6 % to 57.75% and altered the wettability towards water-wet (see Table 11). Likely, the hydrophilic NPs built a layer on the intermediate-wet surface, creating water-wet pores and thus changing the wettability towards water-wet state; this is evidenced by the low contact angle values attained. Moreover, high concentration of NPs in the vicinity of three phase contact region tend to make a thin wedge film, which leads to developing of structural disjoining pressure and spreading of nanoparticles on the surface.

The nanoparticles create new surface layers, overcoming the primary wetting properties of the surface rock. The highest contact angle reduction was recorded for water with the lowest salinity (distilled water), whilst the lowest contact angle reduction occurred for synthetic seawater. In all cases, higher oil recovery is expected due to the lower contact angle. Figure 11 compares the obtained contact angles with and without the presence of NPs in the intermediate-wet system.

Oil-Wet System: Introduction of NPs to the oil-wet system resulted in smaller contact angles than in previous case of intermediate-wet system. It seems that nanoparticles can destabilize oil films on the oil-wet surface and promote the desorption of oil drops. The departure of oil drops from the surface result in changing the wettability towards intermediate-wet state. Structural disjoining pressure could be reason behind the contact angle reduction. Interestingly, the largest contact angle reduction was recorded for distilled water, which is similar to the case of intermediate state. The lowest reduction occurred with the aqueous phase with 5000ppm of TDS. For the brine at 38318ppm, the change in contact angle was quite similar to that observed with water at 5000ppm salinity (see Table 12). Figure 12 compares the recorded contact angles with and without the presence of NPs

Table 10. Reduction of IFT due to the NPs Effect

NPs Concentration (wt%)	TDS (ppm)	Equilibrium IFT (mN/m)	Change in IFT (%)
0	0	17.64	-48.75
0.1	0	9.04	
0	5000	12	-42.66
0.1	5000	6.88	
0	38318	8.38	-51.19
0.1	38318	4.09	

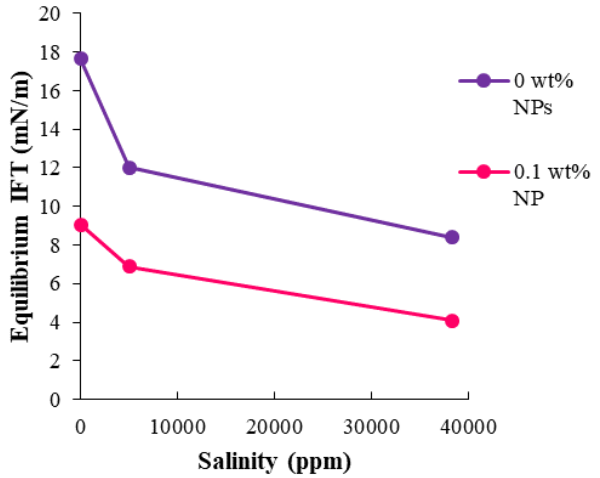

Figure 8. Interfacial tension versus salinity.

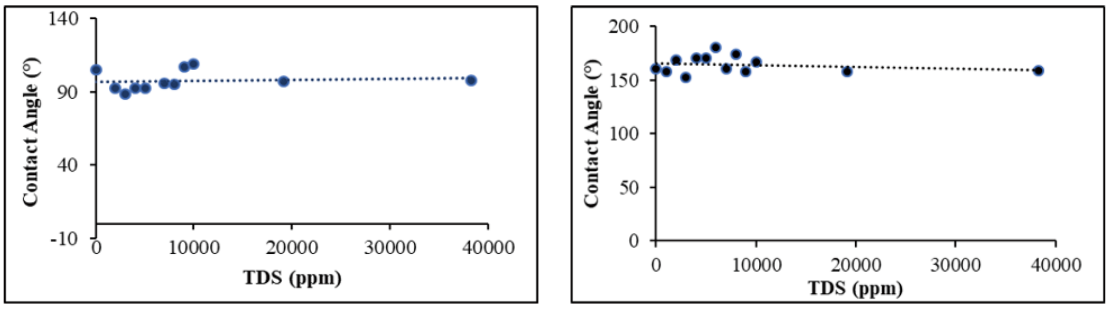

A B

Figure 9. Contact angle vs brine concentration (0-38318 ppm), A intermediate-wet system; B oil-wet system.

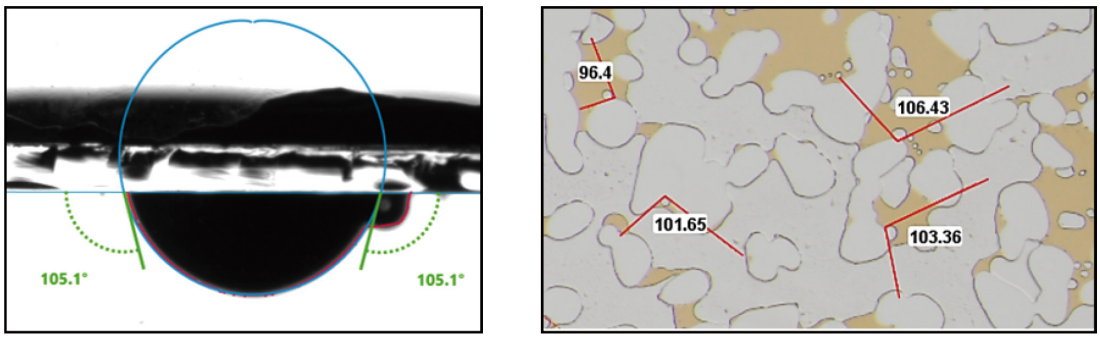

A B

Figure 10. Contact angle measurement in the intermediate-wet system A glass substrates, crude oil and distilled water B microchip flooded with distilled (brown is crude oil).

Table 11. Reduction of Contact Angle due to the NPs Effect in the Intermediate-wet System

NPs Concentration (wt%)	TDS (ppm)	Contact Angle (°)	Change in CA (%)
0.0	0	105.1	-57.75
0.1	0	44.4	
0.0	5000	92.4	-43.72
0.1	5000	52	
0.0	38318	97.4	-38.6
0.1	38318	59.8	

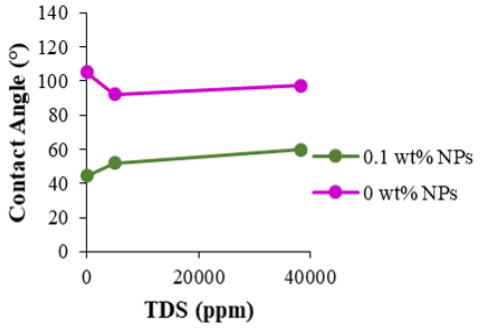

Figure 11. contact angle vs salinity.

Table 12. Reduction of Contact Angle due to the NPs Effect in the Oil-Wet System

NPs Concentration (wt%)	TDS (ppm)	Contact Angle (°)	Change in CA (%)
0	0	160.9	-50.77
0.1	0	79.2	
0	5000	170.7	-45.34
0.1	5000	93.3	
0	38318	158.6	-46.21
0.1	38318	85.3	

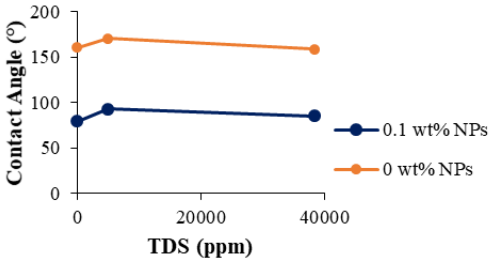

Figure 12. Contact angle variation due to the presence of NPs in the aqueous phase.

in the oil-wet system.

Water-Wet System: The influence of nanoparticles at concentration of 0.1wt% on the contact angle in the water-wet system was also evaluated. A notable reduction in the contact angle was observed for all systems with different salinities. Table 13 shows how contact angle is varied due to the presence of NPs at ambient conditions and Figure 13 shows the graphical representation of these values. Overall, introduction of NPs to the water-wet system reduced the contact angles independent of TDS. The highest reduction is 43.3% which occurs in system with TDS of 5000ppm. On the other hand, when the aqueous phase was distilled water the lowest reduction in contact angle was recorded at 25.76%.

According to the previous studies, the observed trend ties well with a study by Li et al. (2013)[25]. Li et al. measured the contact angle of crude oil against nanofluids (0.1wt%) on water wet glass surface and the reported an angle of 22°.

Table 13. Reduction of Contact Angle due to the NPs Effect in the Water-Wet System

NPs Concentration (wt%)	TDS (ppm)	Contact Angle (°)	Change in CA (%)
0	0	59.81	-25.76
0.1	0	44.4	
0	5000	45.2	-43.3
0.1	5000	25.63	
0	38318	44.9	-41.2
0.1	38318	26.4	

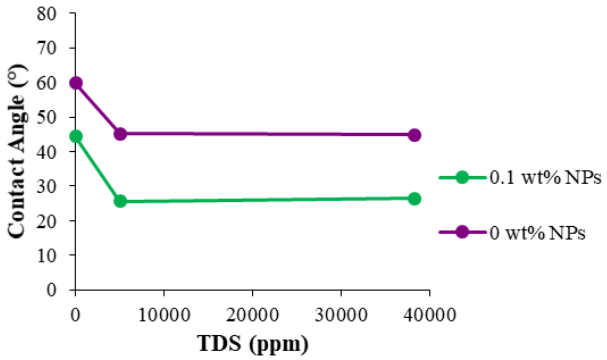

Figure 13. Contact angle variation due to the presence of NPs in the aqueous phase.

However, in the absence of NPs in the aqueous phase (3wt% NaCl) the recorded contact angle increased to 54°. Li et al. evoked the effect electrostatic repulsion force between the NPs to explain the observed reduction in contact angle. As the electrostatic repulsion forces between the NPs strengthens, the nanofluid spreads over the glass surface, resulting in smaller contact angle[26].

3.3 Evaluation of Secondary EOR Flood on Micromodels

In this study, the oil recovery evaluation tests were carried out in the secondary recovery mode, using water-wet, intermediate-wet and oil-wet microchips at ambient conditions. This section discusses how and why salinity variation and the presence of NPs in the injection fluid can increase the recovery factor as a percentage of the initial oil in place. More importantly, these experiments enabled a real-time observation of fluid flow in the porous media, a key aspect towards the understanding of the oil drive mechanisms.

3.3.1 Evaluation of LSWF and Nanofluid Oil Recovery Factor

After performing secondary flooding, a comparison was made between the obtained ultimate oil recoveries (%OOIP). First let us evaluate oil recovery as a function of displacing phase salinity. Figure 14 shows that during water-flooding with different TDS, more oil has been produced from water-wet microchips compared with in intermediate and oil-wet systems. An exception was observed when using water with TDS of 5000ppm. At this salinity, more oil was recovered from intermediate-wet system. Interestingly, at 5000ppm, a smaller contact angle was recorded in comparison with other salinities. After water flooding an oil wet system, oil remains trapped in the smaller pores; Consequently, the ultimate oil recovery was lower than in other wettability states (see red bars in Figure 14).

In the next step NPs (0.1wt%) were added to the displacing phase, the resulting nanofluid system was injected into microchip as secondary EOR fluid. As shown in Figure 15, nanofluids produced extra oil in all systems with different wettability and the oil recovery enhancement ranged between 4.4% to 19.5% of OOIP. The minimal and maximum effect of NPs in improving oil recovery can be observed in the water-wet and oil-wet system, respectively. Thus, the following sections attempt to explain the underlying mechanisms of low salinity water flood augmented silica nanoparticles.

3.3.2 Effect of IFT on Oil Recovery Factor

Previously, over a range of 0 to 10000ppm, and 0 to 38318ppm, we introduced 5000ppm and 38318 respectively as salinity at which the lowest value for interfacial tension occurred. However, these optimum salinities did not correlate with higher oil recovery factor in water-wet and oil-wet system, and no certain trend was observed between the value of IFT and oil recovery. This is not unexpected, because the interfacial tension needs to be decreased orders of magnitudes to improve oil recovery factor considerably, which is not the case. For example, the yield oil recovery factors in water-wet microchip, and IFT versus water

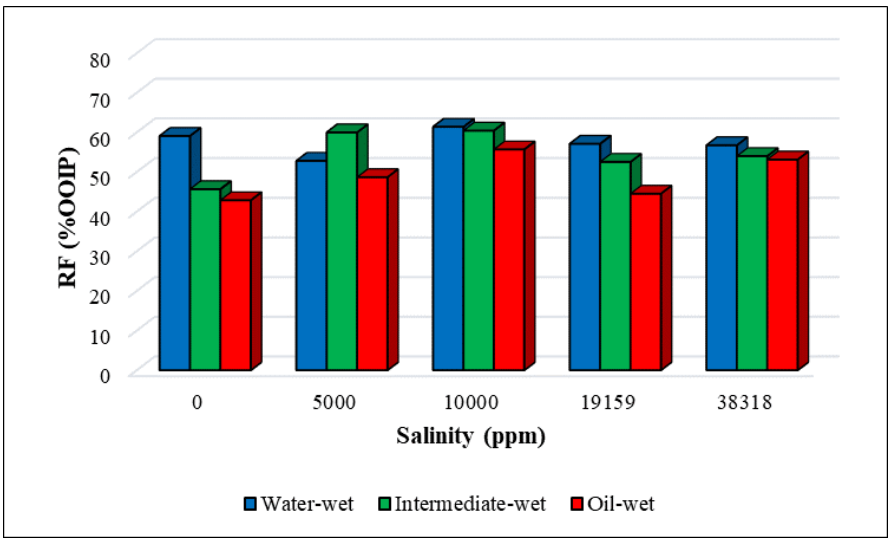

Figure 14. Comparison of oil recovery from water-wet, intermediate-wet, and oil-wet microfluidic chips, using plain water with different TDS.

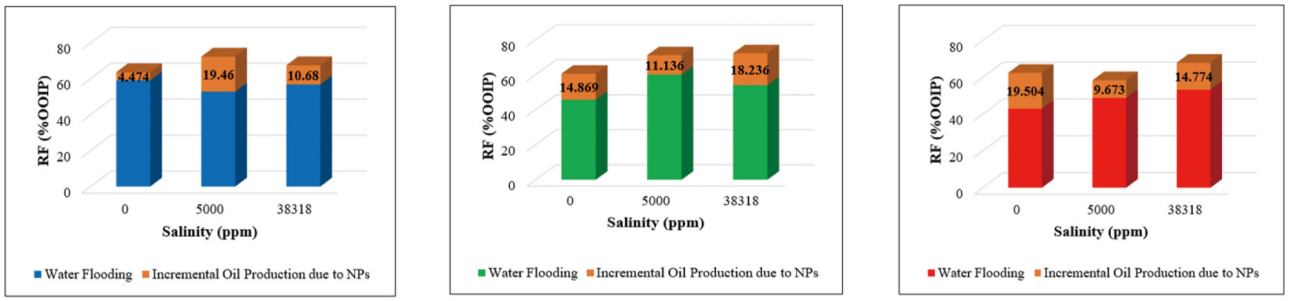

A B C

Figure 15. Comparison of oil recovery from A water-wet; B intermediate-wet, and C oil-wet microfluidic chips, using nanofluids (0.1wt%) with different TDS.

salinity are mapped in Figure 16. For a low salinity range and in the intermediate-wet system, the lowest IFT is achievable at 5000ppm and shows an agreement with the highest oil recovery observed in this work.

The presence of NPs decreased the interfacial tension up 51% (when NPs was dissolved in SSW). The highest reduction in IFT only correlates with the highest recovery factor in the intermediate-wet system (see part (A) of Figure 15), unlike in the case of the oil-wet and water-wet cases. In summary, the IFT reduction played an auxiliary role in improving the oil displacement efficiency microscopically, but perhaps it is not the main oil driving mechanism for low salinity water injection nor for nanofluid injection due to the insufficient ability to decrease IFT to ultra-low values.

3.3.3 Effect of Wettability on Oil Recovery

First, let us inspect the obtained recovery factor (% OOIP) as a function of contact angle in the intermediate-wet system. According to the results obtained in this work, regardless of salinity, all systems remained intermediate-wet. Consequently, no definite trend between contact angle variation and ultimate oil recovery was observed. However, at 5000 ppm, the low contact angle correlates with high oil recovery. In the oil-wet system, the amount of TDS in the water did not affect the measured contact angles enormously and all glasses remained completely oil-wet. Hence, the obtained recovery factors did not correlate with the contact angles. In the intermediate- wet system, introducing NPs to the water reduced all contact angles remarkably towards more water-wet (see Table 11); in this case, the ultimate oil recovery increased in all cases with different salinities (see Figure 17A).

It appears that the main reason behind oil recovery improvement in the presence of NPs is the wettability alteration from intermediate- to more water-wet state. Considering the impact of NPs in the oil-wet system, the wettability was altered to intermediate-wet (see Table 12). Predictably, more oil was recovered during nano flooding in the oil-wet microchips (Figure 17B).

The mechanism of wettability alteration due to the presence of silica nanoparticles can be ascribed to the

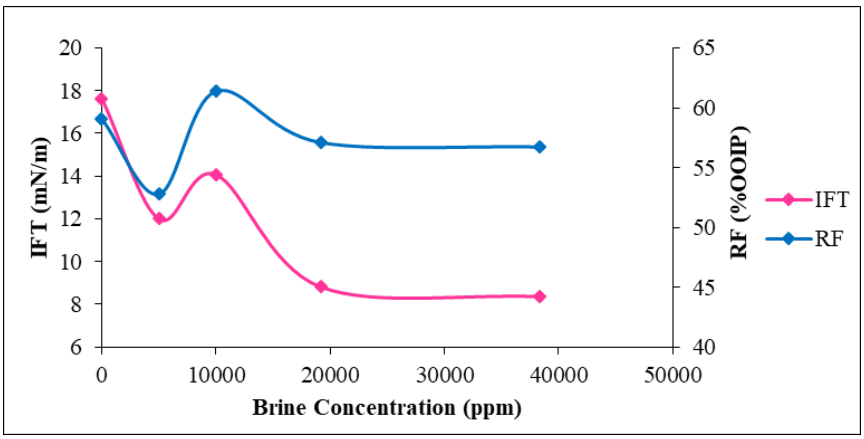

Figure 16. Variation of the IFT and oil recovery factor as a function of salinity in the water- wet system.

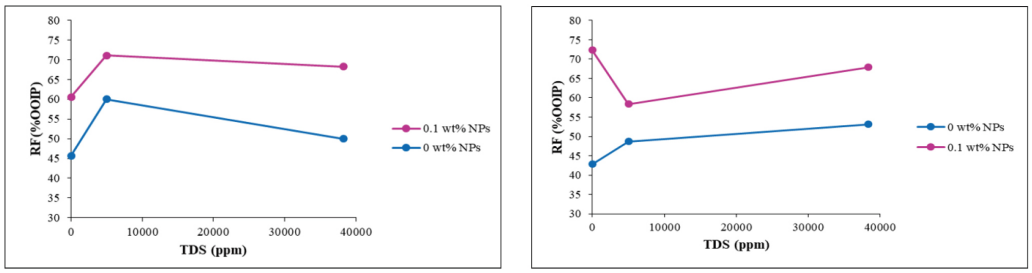

A B

Figure 17. Effect of nanoparticles on the oil recovery factor in the intermediate-wet system (left) and in the oil-wet system (right).

adsorption of NPs onto the surface. In other words, when silica nanoparticles available in the nanofluid medium face the charged surface, due to the charge interactions, the NPs adhere to the surface, creating new surface roughness. This interaction disrupts and detaches the currently absorbed oil molecules to the surface and renders the surface more water-wet[27].

Finally, for the originally water-wet glass, the contact angles remained in the strongly water-wet range, regardless of the salinity content. When adding NPs to the water, contact angle reduction was observed but the systems were still water-wet. The oil recovery improvement was recorded during nanofluid flooding in all cases (see Figure 18). Due to the hydrophilic nature of the silica NPs, their contact with the water-wet surface can reduce contact angles. In fact, NPs tend to confine themselves in the three phase contact line and form a wedge film between water-oil-glass contact line. This NPs concentration-dependent confinement can make the surface even more water-wet[6].

3.3.4 Effect of Viscosity

The viscosity of the injected fluid can influence the oil displacement. Better oil sweep efficiency can be achieved by using a viscous displacing phase, because it leads to compact and evens the moving front and the viscous fingering is minimized[27]. In this study the effect of total dissolved solids and nanoparticles on the water viscosity was monitored at ambient condition (see Table 5 and Table 8). No major effect by salinity or NPs on viscosity was observed, and thus the viscosity effect may not support oil recovery improvement.

3.3.5 Real-time Visualization of Fluid Flow through Micromodel

Fluid flow pattern in the porous media can be governed by wettability state of the system. Figure 19 through Figure 21 show the multiphase flow in three different wettability systems. It is worth to mention that in this study the flow rate was constant in all experiments (0.1µl/min). This means that, in the case of oil production by low displacement fluid flow rate injection, the viscous forces are negligible[28]. All experiments were run for eight hours averaged until residual oil remained constant over time.

Figure 19 shows residual oil saturation in water-wet glass surfaces after the flooding process. The microchip was initially saturated with SSW and crude oil. Then, the system was flooded with synthetic sea water. Figure 19 shows a piston-like displacement trend of crude oil by synthetic seawater. It seems that the displacing phase (synthetic sea water) is moving through the smaller pores, leaving crude oil (non-wetting phase) behind, in the larger pores. For instance, the red circle in subfigure (f) demonstrates the by-

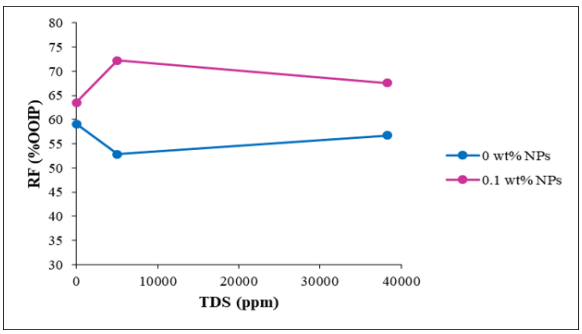

Figure 18. Effect of NPs on oil RF in the water-wet system.

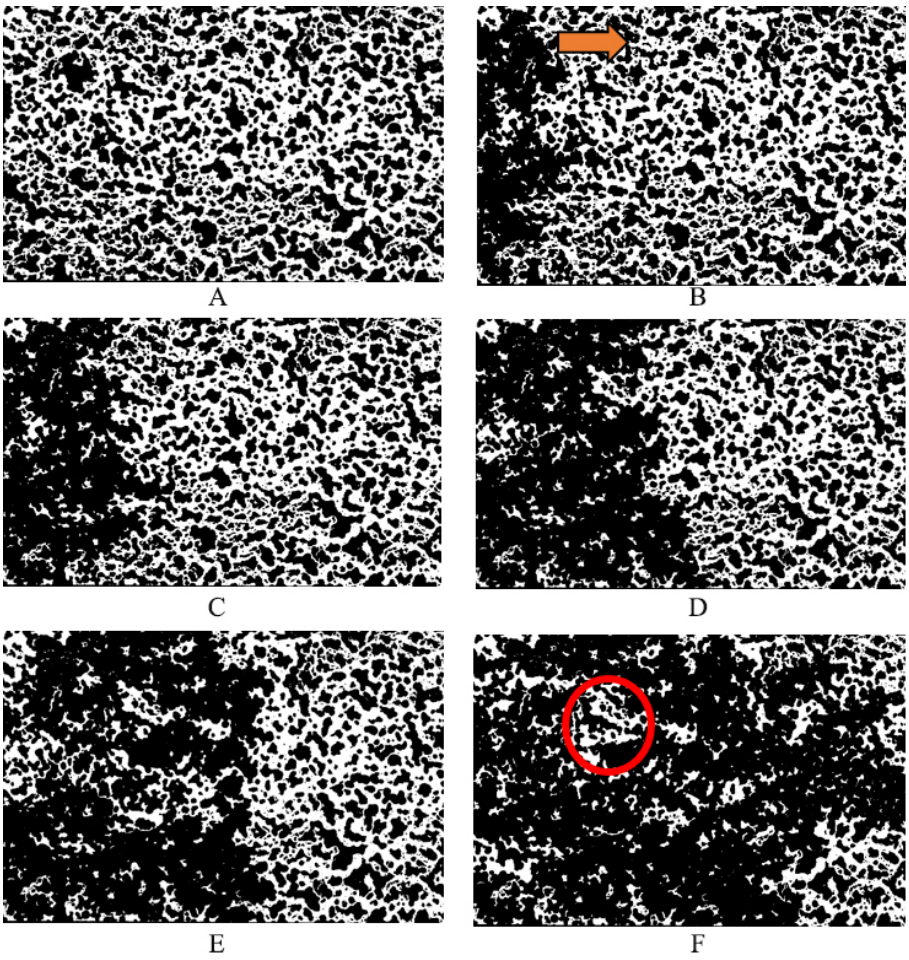

Figure 19. A Water-wet chip saturated with crude oil and SSW at time zero B After 5.34 minutes of injection C After 10.68 minutes D After 21.36 minutes E After 32.04 minutes F After 64.08 minutes (black area is water and glass, white area illustrates the oil and the arrow shows the direction of the injected fluid).

passed oil remained in the larger pore spaces. In fact, since the pore walls are water-wet, low threshold capillary pressure is required for the invading phase to enter small pores. Moreover, the observed displacement pattern is close-packed because the invading fluid (synthetic seawater) can make a strong contact with the water-wet surface. Such a stable displacement can lead to efficient oil recovery. Zhao et al also reported a compact displacement pattern during imbibition[29].

Figure 20 shows the flooding process for an intermediate-wet microchip, initially saturated with SSW and crude oil. This system was also flooded with synthetic sea water. The observed pattern is not stable or compact compared with water-wet system and displacement pattern is capillary fingering. No water invasion is observed in some part of the porous media. For instance, the red circle in subfigure F of Figure 20 shows that water has not swept the trapped oil in the smaller pores. This is because of the less water-wet pore walls, which make the entrance of displacing phase to the small pores more difficult. This difficulty is because higher threshold capillary pressure is needed.

Fluid flow was also recorded in the oil wet system which was initially saturated with synthetic water and crude oil.

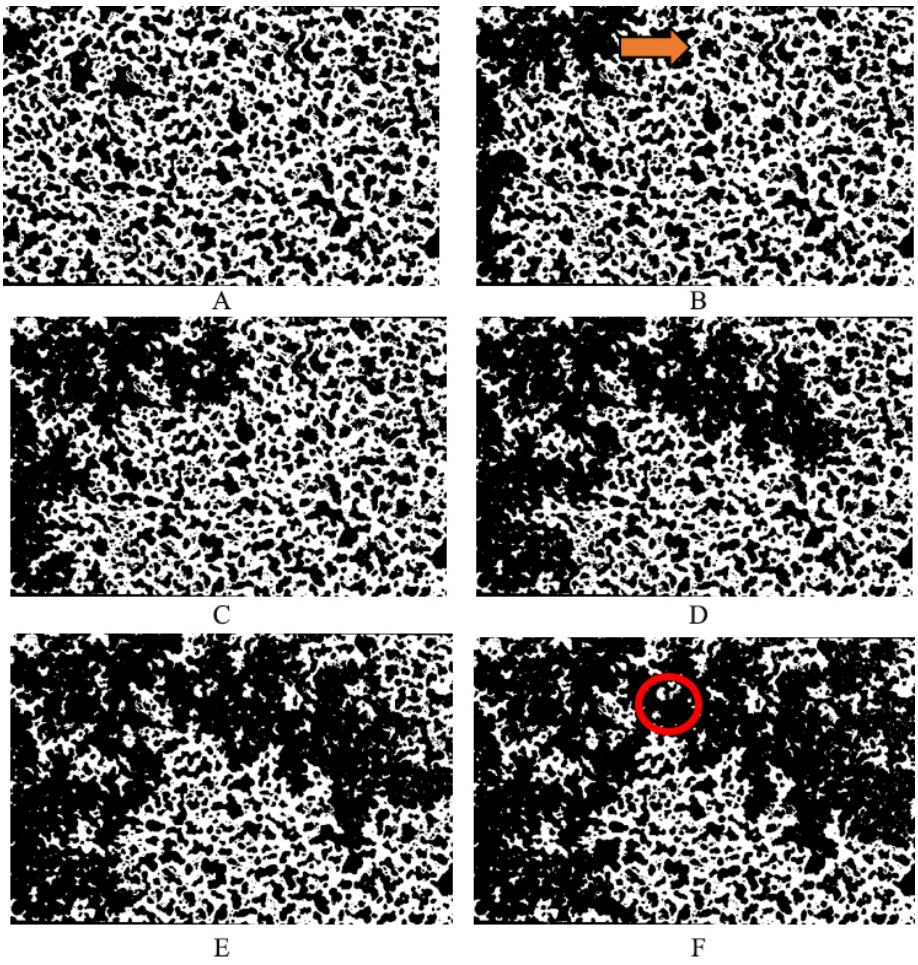

Figure 20. A Intermediate-wet chip saturated with crude oil and SSW at time t =0; B) After 5.34 minutes of injection C After 10.68 minutes D After 21.36 minutes E After 32.04 minutes F After 64.08 minutes (black area is water and glass, white area shows the oil and the arrow highlights the direction of the injected fluid).

Figure 21 illustrates how the non-wetting phase (synthetic seawater in this case) is displacing wetting phase (crude oil) over time. Synthetic seawater (non-wetting fluid) percolates through larger pores easily. In fact, the non-wetting phase can only flow in the bulk of the channels and the wetting phase remains in the extreme corners[28]. On the contrary due to high threshold capillary pressure, it is not easy for the invading phase to sweep oil from small pores, which leads to capillary fingering pattern.

4 CONCLUSION

Fluid flow at the pore scale is mainly governed by capillary forces; In the study, the effect of brine concentration and the nanoparticles on interfacial tension between crude oil and aqueous phase, and wettability states was investigated over a wide range of salinity. The goal was to acquire a better understanding of proposed microscopic mechanism for low salinity augmented silica nanoparticles at microscale. The key findings from this study are summarized below:

(1) LSWF and its diluted samples showed poor oil recovery performance in oil-wet chips, while more oil was produced from water-wet systems.

(2) For the intermediate-wet system, when the salinity of the displacing phase was 5000 ppm, the highest amount of oil was recovered, even more than that obtained from the water-wet chip.

(3) IFT between synthetic seawater (38318 ppm) and crude oil was fairly low, which might be due to asphaltene and resins content and high TAN in the used crude oil.

(4) The wettability (originally water-wet) of glass substrates and microfluidic chips was altered towards intermediate-wet and oil-wet by using hydrocarbon-soluble siliconizing fluid. Contact angle measurements proved the reliability of the utilized method for wettability alteration.

(5) Low salinity water did not change the contact angles dramatically at ambient condition.

(6) The synergic effect of IFT and wettability alteration can be the main oil recovery mechanism in waterflooding with different TDS in intermediate-wet and oil-wet system.

(7) In the water-wet system there is no clear trend between oil recovery, IFT and contact angle reduction.

(8) Silica nanoparticles showed strong affinity towards the surface and reduced contact angles remarkably in all three-wettability state. In fact, the oil-wet system shifts toward intermediate, and the intermediate-wet glass surface became water-wet. Even in the water-wet system, smaller contact

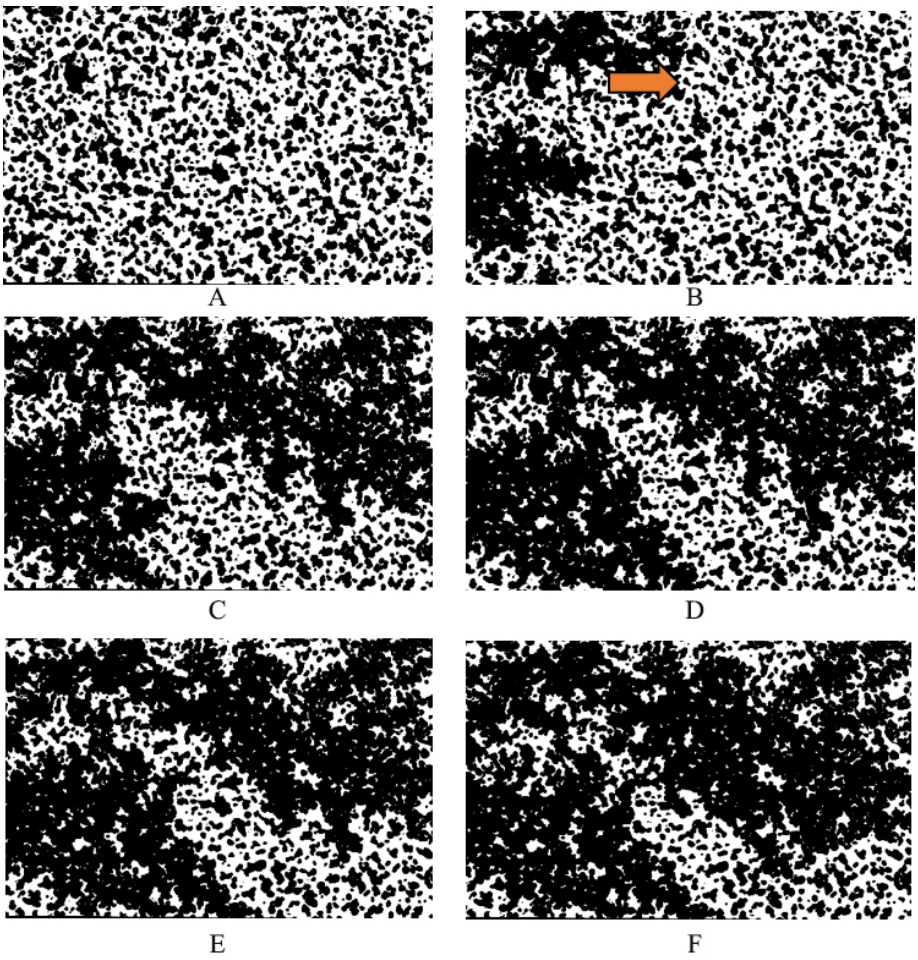

Figure 21. A Oil-wet chip saturated with crude oil and SSW at time t =0; B After 5.34 minutes of injection; C After 10.68 minutes; D After 21.36 minutes; E After 32.04 minutes; F After 64.08 minutes (black area is water and glass, white area is representative of oil and the arrow shows the direction of the injected fluid).

angles were recorded.

(9) During nanofluid flooding, oil recovery enhancement was observed in all systems, (water-wet, intermediate-wet, and oil-wet) and it was varying between 4.4% to 19.5%, depending on the TDS of water.

(10) The combination of nanoparticles and low salinity water increased the oil recovery in all cases. In the water-wet system the synergistic effect of NPs and optimum salinity (5000 ppm) improved oil recovery significantly.

(11) In the oil-wet system the combination of NPs and distilled water resulted in the most efficient oil displacement.

(12) The underlying mechanisms behind oil recovery was nanoparticles adsorption on the surface and wettability alteration. IFT reduction can also mobilize residual oil, but it was not the main mechanism itself.

(13) Multiphase flow pattern in the microfluidic chips was influenced by wettability. In the water-wet chips, the displacement was relatively uniform and compact, while the observed pattern in the intermediate-wet and oil-wet system was not stable and compact. Some sections of the porous media in the intermediate and oil-wet chips, remained uninvaded.

(14) The effect of brine concentration and nanoparticles on the water viscosity was negligible, and thus insufficient to support oil recovery improvement.

Acknowledgements

The authors acknowledge Evonik Industries for providing the nanomaterials and for the technical support and PoreLab, Centre of Excellence grant number 262644, Trondheim-Norway for financial support. We also would like to thank the Centre of Studies in Oil and Gas Engineering and Technology, Eduardo Mondlane University, NUIT: 500003545, Mozambique.

Conflicts of Interest

The authors declare no conflict of interest.

Author Contribution

Conceptualization, methodology, investigation, and writing the manuscript, Safarzadeh S, writing and review of the manuscript Bila A and Torsæter O, Supervision Bila A and Torsæter O.

Abbreviation List

AERODISP®, Aqueous dispersion of hydrophilic silica

nanoparticles produced by Evonik Industries.
AEROSIL®, Hydrophilic silica nanoparticles produced by Evonik Industries.
CA, Contact Angle
EOR, Enhanced Oil Recovery
IFT, Interfacial Tension
LSW, Low Salinity Water
LSWF, Low Salinity Water Flooding
MIE, Multi-component Ion Exchange
NPs, Nanoparticles
OOIP, Original Oil in Place
R, Universal Gas Constant
SSW, Synthetic Seawater
T, Absolute Temperature
TAN, Total Acid Number
TDS, Total Dissolved Solids
μ, Fluid Dynamic Viscosity
σ, Interfacial Tension
dσ, Change in Interfacial Tension
Γi, Surface Excess Concentration
Γi, Surface Excess Concentration

References

[1] UK. BP Amoco. BP Statistical Review of World Energy 2020. Available at https://www.bp.com/content/dam/bp/business-sites/en/global/corporate/pdfs/energy-economics/statistical-review/bp-stats-review-2020-full-report.pdf. Accessed June 2020.

[2] Bernard GG. SPE California Regional Meeting: Effect of Floodwater Salinity on Recovery Of Oil from Cores Containing Clays, Los Angeles, USA, 26-27 October 1967. DOI: 10.2118/1725-MS.

[3] Sheng JJ. Critical review of low-salinity waterflooding. *J Petrol Sci Eng*, 2014; 120: 216-224. DOI: 10.1016/j.petrol.2014.05.026.

[4] Ayatollahi S, Zerafat MM. SPE International Oilfield Nanotechnology Conference and Exhibition: Nanotechnology-assisted EOR techniques: New solutions to old challenges. Noordwijk, The Netherlands, 12-14 June 2012. DOI: 10.2118/157094-ms.

[5] Ding H, Zhang N, Zhang Y et al. Experimental data analysis of nanoparticles for enhanced oil recovery. *Ind Eng Chem Res*, 2019; 58: 12438-12450. DOI: 10.1021/acs.iecr.9b02132.

[6] Wasan DT, Nikolov AD. Spreading of nanofluids on solids. *Nature*, 2003; 423: 156-159. DOI: 10.1038/nature01591.

[7] Skauge T, Hetland S, Spildo K et al. SPE Improved Oil Recovery Symposium: Nano-sized particles for EOR. Tulsa, USA, 24-28 April 2010. DOI: 10.2523/129933-ms.

[8] Chevalier Y, Bolzinger MA. Emulsions stabilized with solid nanoparticles: Pickering emulsions. *Colloids Surfaces A Physicochem Eng Asp*, 2013; 439: 23-34. DOI: 10.1016/j.colsurfa.2013.02.054.

[9] Hendraningrat L, Torsæter O. A study of water chemistry extends the benefits of using silica-based nanoparticles on enhanced oil recovery. *Appl Nanosci*, 2016; 6: 83-95. DOI: 10.1007/s13204-015-0411-0.

[10] Ebrahim T, Mohsen VS, Mahdi SM et al. Performance of low-salinity water flooding for enhanced oil recovery improved by SiO2 nanoparticles. *Petrol Sci*, 2019, 16(2): 357-365. DOI: 10.1007/s12182-018-0295-1.

[11] Dehaghani AHS, Daneshfar R. How much would silica nanoparticles enhance the performance of low-salinity water flooding?*Petrol Sci*, 2019; 16: 591-605. DOI: 10.1007/s12182-019-0304-z.

[12] Gaol CL, Wegner J, Ganzer L. Real structure micromodels based on reservoir rocks for enhanced oil recovery (EOR) applications. *Lab Chip*, 2020; 20: 2197-2208. DOI: 10.1039/d0lc00257g.

[13] R. Zwiers. Micronit. *Glass*, no. November, 2007; 1-16.

[14] McCartney RA, Rein E. Tekna's 16. international oil field chemistry symposium: Formation waters of the Norwegian Continental Shelf, Geilo, Norway, 13-16 Mar 2005.

[15] Omran M, Akarri S, Torsaeter O. The effect of wettability and flow rate on oil displacement using polymer-coated silica nanoparticles: a microfluidic study. *Processes*, 2020; 8: 991. DOI: 10.3390/pr8080991.

[16] Herd MD, Lassahn GD, Thomas CP et al. SPE/DOE Enhanced Oil Recovery Symposium: Interfacial tensions of microbial surfactants determined by real-time video imaging of pendant drops. Tulsa, USA, 22-24 April 1992. DOI: 10.2118/24206-ms.

[17] USA. Thermo Scientifi. AquaSil™ and SurfaSil™ Siliconizing Fluids. Available at https://www.interchim.fr/ft/2/23080P.pdf. Accessed 2008.

[18] Kruss. Available at https://www.kruss-scientific.com. Accessed 2021.

[19] Bashforth F, Adams JC. An attempt to test the theories of capillary action by comparing the theoretical and measured forms of drops of fluid. University Press: Cambridge, UK, 1883.

[20] Moeini F, Hemmati-Sarapardeh A, Ghazanfari MH et al. Toward mechanistic understanding of heavy crude oil/brine interfacial tension: The roles of salinity, temperature and pressure. *Fluid Phase Equilibr*, 2014; 375: 191-200. DOI: 10.1016/j.fluid.2014.04.017.

[21] Rajagopalan R, Hiemenz PC. Principles of colloid and surface chemistry. Marcel Dekker, Inc: New York, USA, 1997.

[22] Kumar B. Effect of salinity on the interfacial tension of model and crude oil systems [master's thesis]. Calgary, Alberta: University of Calgary; 2012. DOI: 10.11575/PRISM/25807.

[23] Lashkarbolooki M, Ayatollahi S, Riazi M. Effect of salinity, resin, and asphaltene on the surface properties of acidic crude oil/smart water/rock system. *Energ Fuel*, 2014; 28: 6820-6829. DOI: 10.1021/ef5015692.

[24] Morrow NR. Wettability and its effect on oil recovery. *J Petrol Technol*, 1990; 42: 1476-1484. DOI: 10.2118/21621-PA.

[25] Treiber LE, Owens WW. A laboratory evaluation of the wettability of fifty oil-producing reservoirs. *Soc Petrol Eng J*, 1972; 12: 531-540. DOI: 10.2118/3526-pa.

[26] Li S, Hendraningrat L, Torsaeter O. IPTC 2013: International Petroleum Technology Conference. Improved oil recovery by hydrophilic silica nanoparticles suspension: 2 phase flow

experimental studies, Beijing, China, 26-28 March 2013. Houten, Netherlands, European Association of Geoscientists & Engineers; 2013. DOI: 10.2523/16707-ms.

[27] Afolabi RO, Yusuf EO. Nanotechnology and global energy demand: challenges and prospects for a paradigm shift in the oil and gas industry. *J Pet Explor Prod Te*, 2019; 9: 1423-1441. DOI: 10.1007/s13202-018-0538-0.

[28] Lenormand R. Liquids in porous media. *J Phys-Condens Mat*, 1990; 2: SA79. DOI: 10.1088/0953-8984/2/S/008.

[29] Zhao B, MacMinn CW, Juanes R. Wettability control on multiphase flow in patterned microfluidics. *P Natl Acad Sci*, 2016; 113: 10251-10256. DOI: 10.1073/pnas.1603387113.